

Numerical modeling of a hybrid GFRP-concrete beam subjected to low-velocity impact loading

†*Z. Li¹, A. Khennane¹, P. J. Hazell¹, and A. Remennikov²

¹School of Engineering and Information Technology, The University of New South Wales, Canberra, Australia.

²School of Civil, Mining and Environmental Engineering, University of Wollongong, Australia.

*Presenting author: zongjun.li@student.adfa.edu.au

†Corresponding author: zongjun.li@student.adfa.edu.au

Abstract

This study reports on the results of a numerical investigation on the impact behaviour of a hybrid GFRP-concrete beam subjected to low-velocity impacts with different impact energy levels. A non-linear finite element model has been developed using the commercial software ABAQUS/Explicit to simulate the impact performance of the hybrid beam under dynamic loading. The numerical results, including the dynamic loading history, failure modes and impact performance are compared to the experimental results. The agreement between the numerical and experimental results indicates that the developed numerical model is capable of analysing the impact behaviour of such hybrid GFRP-concrete system.

Keywords: Numerical modeling, Finite element method, Failure modes, Impact performance

Introduction

Fiber reinforced polymer (FRP) composite materials have been extensively used due to their excellent anti-corrosion performance. Composite materials in the form of pultruded glass fiber reinforced polymer (GFRP) profiles have a great potential since they are economically affordable through the pultrusion process, which offers the best productivity/cost ratio of all the composites fabrication processes [1]. However when used as structural elements on their own, pultruded profiles suffer from the susceptibility to instability, the high deformability and the brittle failure [2][3]. On the other hand, when combined in a hybrid form with concrete, they have shown to offer excellent performance as floors [4], bridge decks [5][6], beams [7]-[11], and rail sleepers [12] when subject to static loadings.

However, their dynamic performance has yet to be assessed. If these hybrid beams are to be used as bridge girders or railway sleepers, their impact behavior has to be investigated. The aim of this study therefore is to investigate the behavior of a hybrid beam made of a rectangular hollow pultruded profile filled with concrete using a numerical model because experimentation alone does not reveal the failure modes of the concrete hidden inside the pultruded profile. For this purpose, the numerical investigation will help to analyse the development and propagation of damage in the concrete.

Experimental program

To verify the numerical modeling of the hybrid GFRP-concrete beam, the experimental tests of this hybrid beam are reported briefly here. Six hybrid beams, which consisted of rectangular hollow section pultruded GFRP profiles filled with high performance concrete, were tested along the weak axis. The hybrid beams were subjected to a concentrated impact load by a cylindrical impactor for three ascending impact energy levels. The total length and the span length of each beam is 2000 mm and 1440 mm respectively. The schematic diagram of the test setup is shown in Fig. 1.

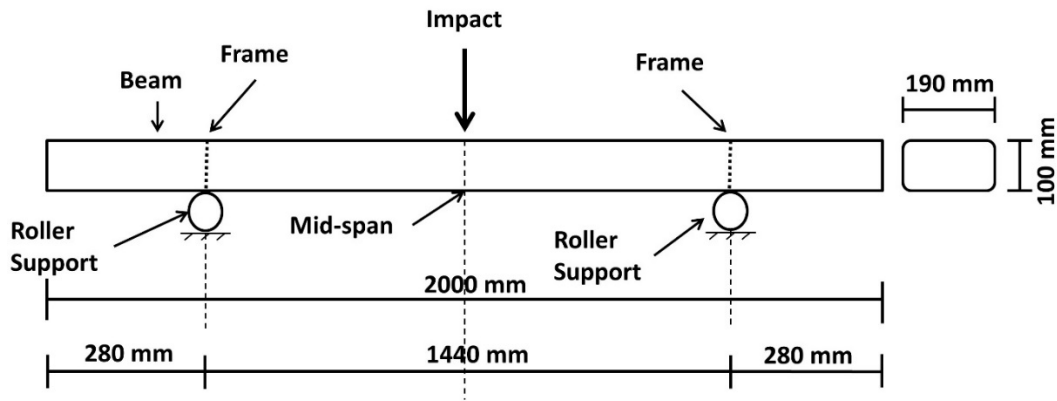


Figure 1. Schematic diagram of experimental setup

Numerical modeling

Finite element method

The experimental results can only provide the impact characteristics and performance for the hybrid GFRP-concrete beam. Details such as concrete damage or debonding between the concrete block and the pultruded profile are not visible. For this purpose, a non-linear finite element (FE) model was developed using the commercial software ABAQUS/Explicit to study these phenomena and predict the overall response of the hybrid GFRP-concrete beam subjected to low-velocity impacts. The impactor was modeled using discrete rigid elements (R3D4). A mass of 592 kg was assigned to the impactor as per experimental conditions. The concrete block is modelled using linear eight-node three dimensional solid elements with reduced integration (C3D8R). As reported in Li et al. (2017), the through-thickness properties of pultruded GFRP composites are negligible in low-velocity impact cases, therefore all the effective layers of the GFRP composites were modeled by using eight-node quadrilateral in-plane general-purpose continuum shell elements (SC8R) [13]. The orientation of the fibers in each layer was assigned accordingly to the corresponding coordinate systems. The mesh density was chosen to 20 mm \times 20 mm for the hybrid beam members on the basis of mesh sensitivity analysis in terms of computational time and convergence solution. Three different initial impact velocities were imposed to the impactor to simulate the impact events. The boundary conditions are shown in Fig. 2 according to the experimental setup. The interaction between the impactor and the hybrid beam was simulated by surface-to-surface contact pairs. The mechanical constraint formulation was enforced using the kinematic contact algorithm, and the friction coefficient was set to 0.5. The interaction between the pultruded profiles and the concrete was also simulated by surface-to-surface contact pairs but with 0.3 as the friction coefficient factor.

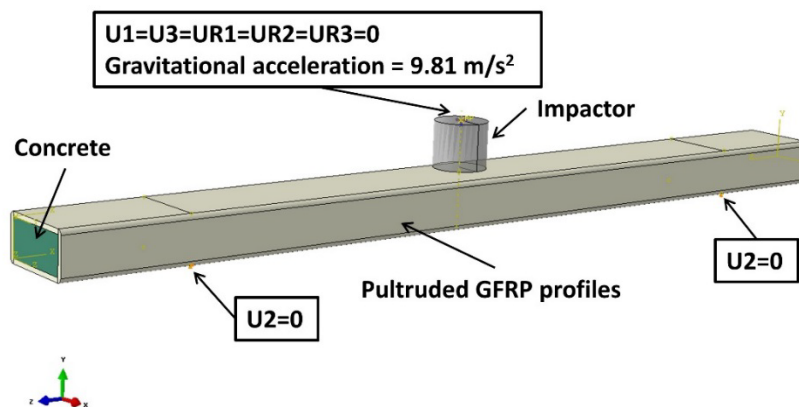


Figure 2. Assembled FE model with boundary conditions

Material models

Two material models of high performance concrete and pultruded GFRP composites were used in this study. The concrete section of the hybrid beam was modeled by the use of concrete damaged plasticity model (CDPM) and, the pultruded profiles were modeled using the FRP composite material model (Hashin damage model). For the compressive behaviour of concrete, two stress-strain relationship models were used to represent the ascending and descending zone respectively. The expression developed by Popovics (1973), modified by Thorenfeldt et al. (1987), were used to describe the compressive hardening behaviour (ascending zone), as shown in Eq. (1) [14][15].

$$\frac{f_c}{f_c'} = \frac{\varepsilon_c}{\varepsilon_c'} \cdot \frac{n}{n-1 + \left(\frac{\varepsilon_c}{\varepsilon_c'}\right)^{nk}} \quad (1)$$

The expression proposed by Wee et al. (1996) was used to describe the strain softening behaviour (descending zone), as shown in Eq. (2) [16].

$$f_c = f_c' \left\{ \frac{k_1' \beta \left(\frac{\varepsilon_c}{\varepsilon_c'}\right)}{k_1' \beta - 1 + \left(\frac{\varepsilon_c}{\varepsilon_c'}\right)^{k_2' \beta}} \right\} \quad (2)$$

The tension stiffening behaviour of the concrete was defined with the post-failure stress as a function of cracking strain in this study. The compressive and tensile stress-strain curves, shown in Fig. 3 and Fig. 4, were implemented in CDPM.

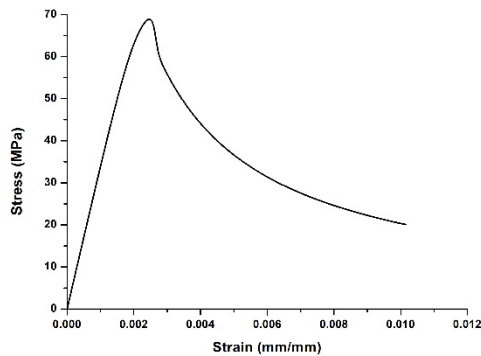


Figure 3. Compressive stress-strain curve

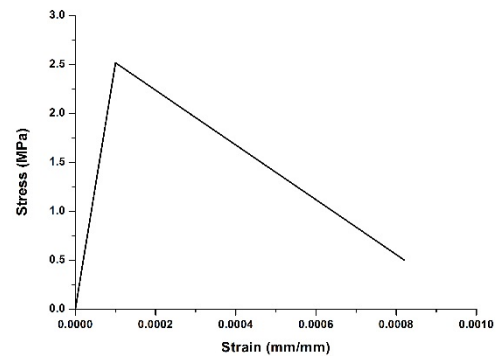


Figure 4. Tensile stress-strain curve

The FRP damage model for fiber-reinforced composites were used to predict the onset of failure and post-failure development of the pultruded GFRP profiles. Details of mechanisms of CDPM and fiber-reinforced material model can be found in ABAQUS documentation [17]. The material properties and input parameters are shown in Table 1-4 below.

Table 1. Material properties of pultruded GFRP profiles [13]

$E_1 [MPa]$	$E_2 [MPa]$	$G_{12} = G_{13}^* = G_{23}^* [MPa]$	ν_{12}	$\varepsilon_f^T = \varepsilon_f^{C^*}$	$\varepsilon_t^T = \varepsilon_t^{C^*} = \varepsilon^{S^*}$
28870	3505	2980	0.21	0.011	0.013

Table 2. Damage initiation parameters of pultruded GFRP profiles [13]

X^T [MPa]	X^C [MPa]	Y^T [MPa]	Y^C [MPa]	S^L [MPa]	S^{T*} [MPa]
301.198	310.785	29.78	31.97	33.0	33.0

Table 3. Damage evolution parameters for pultruded GFRP profiles [13]

$G_{ft,c}^*$ [N/mm]	$G_{fc,c}^*$ [N/mm]	$G_{mt,c}^*$ [N/mm]	$G_{mc,c}^*$ [N/mm]
55.0	95.0	11.5	11.5

Table 4. Material properties of concrete

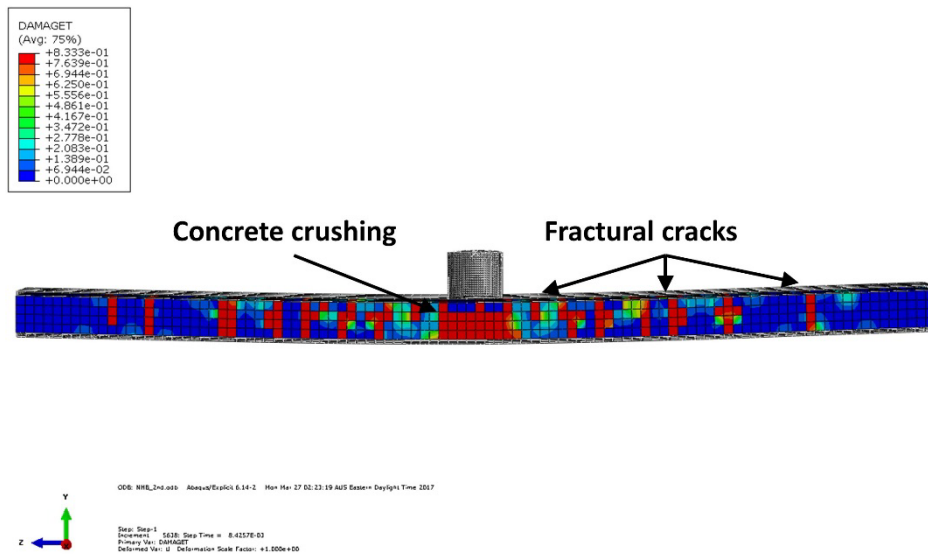
Cross-section, [mm]	Modulus of elasticity, [MPa]	Poisson's ratio	Maximum compressive strength, [MPa]	Maximum tensile strength, [MPa]
170 × 80	33930	0.18	69.84	2.52

*Assumed

Numerical results

Failure modes

The predicted results were compared to the experimental ones. The numerical results identified four main failure modes. Taking the 450 mm dropping height case (impact velocity = 2.97 m/s) as an example, as shown in Fig. 5, localised concrete crushing occurred at the impact area. Moreover, fractural cracks can be found between the mid-span and the supports. The concrete fractured into several parts due to the impact loading. Shear cracks on the corners of the profiles can be observed in both the numerical and experimental results as shown in Fig. 6. The fourth and the last failure mode is the slip of the concrete. Debonding between the concrete and the profiles occurred in both the numerical and experimental results during the tests as shown in Fig. 7.

**Figure 5. Fractural cracks of the concrete inside**

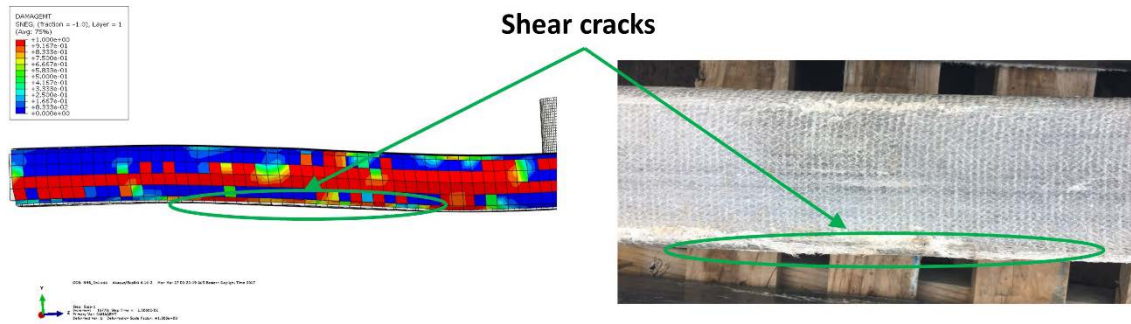


Figure 6. Shear cracks on the corners of the profiles for both numerical and experimental observations

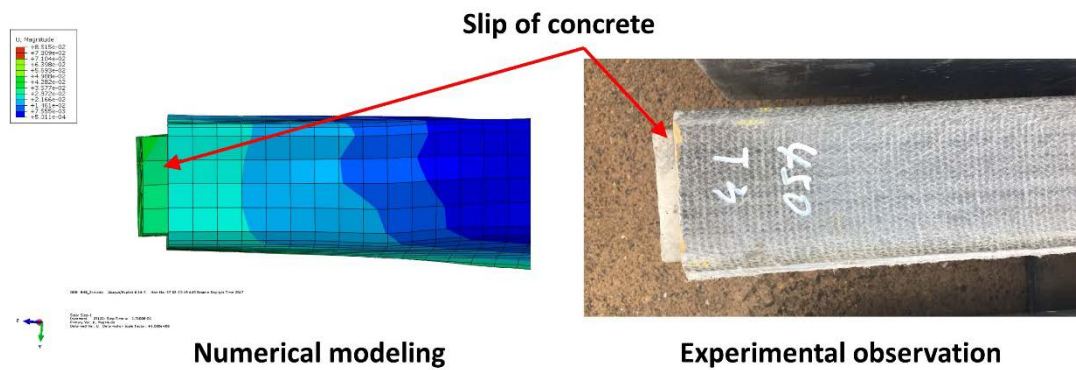


Figure 7. Slip of concrete for both numerical and experimental observations

Loading history and impact performance

The comparisons of the numerical and experimental results for three loading histories are shown in Fig. 8. A reasonably good agreement is achieved between the experimental results and numerical ones. The typical loading histories for all impact energy levels can be divided into two stages, inertial resistance stage and dynamic bending resistance stage. Just after contact is initiated between the impactor and the top surface of the hybrid beam, the first stage is represented by a significant rapid increase in load to the maximum value, and dropping back to zero. In this stage, the impact force is represented by a rapid, short peak of inertial force due to the striking drop mass on the contact zone. The inertial force increases and then decreases quickly as the velocity of the hybrid beam increases. In the numerical prediction, the impactor was modeled as a rigid part instead of a steel impactor. This could explain why the predicted values in this stage are relatively higher than the experimental ones. The true impact resistance of the hybrid beam is represented by the second stage. In this stage, the hybrid beam starts to carry the impact load until failure occurs. Multiple failure mechanisms occur in this stage, including the debonding failure between the concrete and the profiles, shear cracks on the corners of the profiles and the fracture of the concrete. The average maximum experimental impact loads recorded in this stage are 84.8, 100.3 and 110.2 kN, respectively for the three ascending energy levels. The corresponding predicted values are 96.9, 104.9 and 105.5 kN respectively. The average difference between experimental results and numerical ones is only 7%. The numerical predictions are found to corroborate the experimental results in terms of failure modes and impact performance.

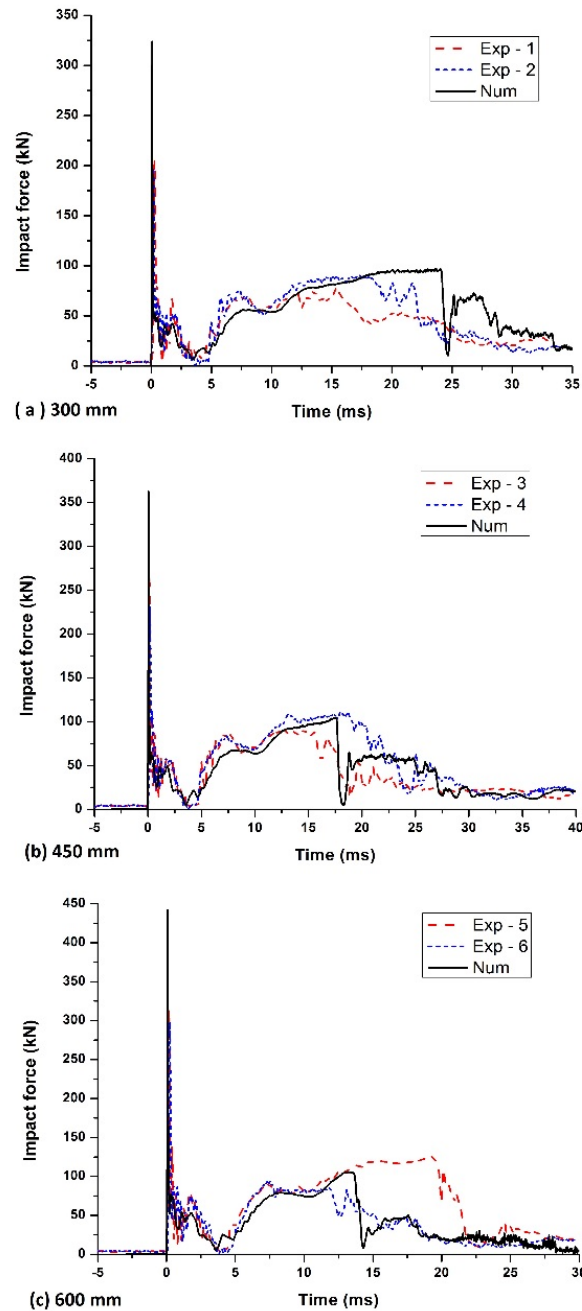


Figure 8. Comparison of loading histories for three ascending energy levels

Conclusions

A numerical investigation of the impact resistance of hybrid GFRP-concrete beams subjected to low-velocity impacts has been conducted. Three dimensional FE models were developed to predict the impact behaviour of this hybrid system. Multi-nonlinear stress-strain relationships were combined to describe the material models. The numerical results including the dynamic loading histories, failure modes and impact performance are compared and verified with the experimental results. The agreement between numerical and experimental results indicates that the developed numerical model is capable of analysing the impact behaviour of hybrid GFRP-concrete systems.

References

- [1] Zureick, K. and Scott, D. (1997) Short-term behavior and design of fiber-reinforced polymeric slender members under axial compression, ASCE, *Journal of Composites for Construction* **1(4)**, 140-149.
- [2] Correia, J. R., Branco, F. A. and Ferreira, J. G. (2007) Flexural behaviour of GFRP-concrete hybrid beams with interconnection slip, *Composite Structures* **77(1)**, 66-68.
- [3] Gonilha, J. A., Correia, J. R. and Branco, F. A. (2013) Dynamic response under pedestrian load of a GFRP-SFRSCC hybrid footbridge prototype: Experimental tests and numerical simulation, *Composite Structures* **95**, 453-463.
- [4] Correia, J. R., Branco, F. A. and Ferreira, J. (2009) GFRP-concrete hybrid cross-sections for floors of buildings, *Engineering Structures* **31(6)**, 1331-1343.
- [5] He, J., Liu, Y., Chen, A. and Dai, L. (2012) Experimental investigation of movable hybrid GFRP and concrete bridge deck, *Construction and Building Materials* **26(1)**, 49-64.
- [6] Mendes, P. J. D., Barros, J. A. O., Sena-Cruz, J. M. and Taheri, M. (2011) Development of a pedestrian bridge with GFRP profiles and fiber reinforced self-compacting concrete deck, *Composite Structures* **93(11)**, 2969-2982.
- [7] Deskovic, N., Triantafillou, T. C. and Meier, U. (1995) Innovative design of FRP combined with concrete: short term behaviour, ASCE, *Journal of Structural Engineering* **121(7)**, 1069-1078.
- [8] Canning, L., Hollaway, L. and Thorne, A. M. (1999) Manufacture, testing and numerical analysis of an innovative polymer composite/concrete structural unit, *Proceedings-institution of civil engineers, structures and buildings* **134**, 231-241.
- [9] Hulatt, J., Hollaway, L. and Thorne, A. (2003) Short term testing of hybrid T beam made of new prepreg material, *Journal of Composites for Construction* **7(2)**, 135-144.
- [10] Khennane, A. (2009) Manufacture and testing of a hybrid beam using a pultruded profile and high strength concrete, *Australian Journal of Structural Engineering* **10(2)**, 145-155.
- [11] Chakraborty, A., Khennane, A., Kayali, O. and Morozov, E. (2011) Performance of outside filament-wound hybrid FRP-concrete beams, *Composites Part B: Engineering* **42(4)**, 907-915.
- [12] Ferdous, W., Manalo, A., Khennane, A. and Kayali, O. (2015) Geopolymer concrete-filled pultruded composite beams – Concrete mix design and application, *Cement and Concrete Composites* **58**, 1-13.
- [13] Li, Z., Khennane, A., Hazell, P. J. and Brown, A. D. (2017) Impact behaviour of pultruded GFRP composites under low-velocity impact loading, *Composite Structures* **168**, 360-371.
- [14] Popovics, S. (1973) A numerical approach to the complete stress-strain curve of concrete, *Cement and Concrete Research* **3**, 583-599.
- [15] Thorenfeldt, E., Tomaszewicz, A. and Jensen, J. J. (1987) Mechanical properties of high strength concrete and application in design, *Proceeding of the Symposium of Utilization of high strength concrete*, Trondheim, 149-159.
- [16] Wee, T. H., Chin, M. S. and Mansur, M. A. (1996) Stress-strain relationship of high-strength concrete in compression, *Journal of Materials in Civil Engineering* **8(2)**, 70-76.
- [17] ABAQUS, ABAQUS Documentation, Dassault Systèmes, Providence, RI, USA, 2011.